Reconstruction of Kinetic Parameter Images Directly from Dynamic PET Sinograms

Mustafa E. Kamasak[a], Charles A. Bouman[a], Evan D. Morris[b] and Ken Sauer[c]

[a]School of Electrical and Computer Engineering, Purdue University, West Lafayette, IN;
[b]Indiana University, Purdue University-Indianapolis Radiology and Biomedical Engineering Departments, Indianapolis, IN;
[c]Department of Electrical Engineering, University of Notre Dame, Notre Dame, IN;

ABSTRACT

Recently, there has been interest in estimating kinetic model parameters for each voxel in a PET image. To do this, the activity images are first reconstructed from PET sinogram frames at each measurement time, and then the kinetic parameters are estimated by fitting a model to the reconstructed time-activity response of each voxel. However, this indirect approach to kinetic parameter estimation tends to reduce signal-to-noise ratio (SNR) because of the requirement that the sinogram data be divided into individual time frames. In 1985, Carson and Lange proposed,[1] but did not implement, a method based on the EM algorithm for direct parametric reconstruction. More recently, researchers have developed semi-direct methods which use spline-based reconstruction, or direct methods for estimation of kinetic parameters from image regions. However, direct voxel-wise parametric reconstruction has remained a challenge due to the unsolved complexities of inversion and required spatial regularization. In this work, we demonstrate an efficient method for direct voxel-wise reconstruction of kinetic parameters (as a parametric image) from all frames of the PET data. The direct parametric image reconstruction is formulated in a Bayesian framework, and uses the parametric iterative coordinate descent (PICD) algorithm to solve the resulting optimization problem.[2] This PICD algorithm is computationally efficient and allows the physiologically important kinetic parameters to be spatially regularized. Our experimental simulations demonstrate that direct parametric reconstruction can substantially reduce estimation error of kinetic parameters as compared to indirect methods.

Keywords: tomography, iterative reconstruction, dynamic PET, kinetic modeling, regularization

1. INTRODUCTION

Positron Emission Tomography (PET) is a powerful molecular imaging technique with the sensitivity to detect picomolar quantities of a labelled tracer with reasonable (seconds to minutes) temporal resolution. Through the application of kinetic models, the dynamic PET data can be transformed into physiological parameters that indicate the functional state of the imaged tissue. Kinetic compartmental models are often used to describe the movement of a tracer between different physically or chemically distinct states or compartments.[4] The exchange of tracer between these compartments can be modeled by a system of first order ordinary differential equations (ODEs) whose coefficients are the kinetic parameters. The resulting kinetic models have been validated as producing reliable quantitative indices of various clinically and scientifically important physiological processes[5]

In some cases, a single set of kinetic parameters can describe the tracer behavior in a homogeneous region of tissue. If the region of interest can be delineated using some form of segmentation, then the PET activity can be averaged over the region at each time frame and a single set of kinetic parameters can be estimated by fitting a single kinetic model to the time sequence of average activities. The PET data are first reconstructed into K

Send correspondence to Mustafa E. Kamasak
Mustafa E. Kamasak: E-mail: kamasak@purdue.edu, Telephone: +1 765 496 3717
Charles A. Bouman: E-mail: bouman@ecn.purdue.edu, Telephone: +1 765 494 0340
Evan D. Morris: E-mail: emorris@iupui.edu, Telephone: +1 317 274 1802
Ken Sauer: E-mail: sauer@nd.edu, Telephone: +1 574 631 6999

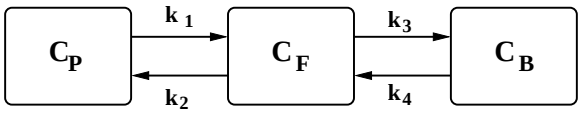

Figure 1. 2 tissue compartment model with 4 kinetic parameters.

time frames, then a region of interest (ROI) is segmented from each frame, and a single set of kinetic parameters is fit to the regional-average time sequence.

Recently, there has been increasing interest in the formation of parametric images which model the kinetic behavior of each voxel individually. This approach is more appropriate when the volume cannot be effectively segmented into homogeneous regions that would be modeled with a single kinetic parameter set. Existing approaches to the creation of parametric images can be roughly categorized as "indirect", "semi-direct", and (our new method) "direct" reconstruction. Indirect methods work by first reconstructing the PET emission images for each of the K measurement times, and then estimating the kinetic parameters at each voxel. Semi-direct algorithms, as they are sometimes named, attempt to improve signal-to-noise by constraining the possible choices of time-courses for each voxel via signal sub-spaces or splines. Ideally, one would like to estimate directly the space-domain kinetic parameters from the measured sinogram data. In fact, Carson and Lange[1] proposed direct estimation of kinetic parameters from PET data in 1985. In that paper, the authors outlined a general framework for a direct reconstruction algorithm based on expectation-maximization (EM) iterations. Unfortunately, the Carson and Lange direct parametric reconstruction algorithm has never, to our knowledge, been fully implemented for nonlinear estimation of a dense set of voxels.

This paper introduces a novel algorithm for directly reconstructing parametric images from PET sinogram data. We demonstrate that this method can generate parametric images with superior quality; and, perhaps surprisingly, we also show that it has computational requirements that are similar to a two-step approach of iterative reconstruction followed by kinetic parameter estimation.

2. 2-TISSUE COMPARTMENT MODEL

In this paper, we used a 2-tissue compartment model to describe the kinetic processes that are represented by the signal from each voxel of a reconstructed image. Figure 1 illustrates the model: C_P (pmol/ml) is the molar concentration of tracer in the plasma, C_F (pmol/ml) is the molar concentration of unbound tracer, and C_B (pmol/ml) is the molar concentration of metabolized or bound tracer. The model depends on the kinetic parameters, k_1, k_2, k_3, and k_4, which specify the tracer exchange rates between compartments in units of inverse minutes. In addition, there are two compound parameter groups that have ready physiological interpretations and practical application, particularly for receptor-ligand imaging: binding potential (BP), and total volume of distribution (VD). BP is proportional to the number of receptors and VD represents the steady state distribution of tracer between the plasma and tissue. BP and VD can be expressed in terms of the aforementioned kinetic parameters, $BP = \frac{k_3}{k_4}$ and $VD = \frac{k_1}{k_2}\left(1 + \frac{k_3}{k_4}\right)$.

In applying the model in Fig. 1 to all voxels, we assume that the delivery of tracer is the same to all regions being imaged. In other words, the value of C_P is not a function of voxel position. However, the values of the kinetic parameters will be allowed to vary for each voxel location, s. Using these assumptions, the time variation of the concentrations for a single voxel are governed by the following ordinary differential equations (ODE).

$$\frac{dC_F(s,t)}{dt} = k_{1s}C_P(t) - (k_{2s} + k_{3s})C_F(s,t) + k_{4s}C_B(s,t) \quad (1)$$

$$\frac{dC_B(s,t)}{dt} = k_{3s}C_F(s,t) - k_{4s}C_B(s,t) \ . \quad (2)$$

In this work, $C_P(t)$ is assumed known. In practice, it can be measured directly from arterial plasma samples during the imaging procedure,[6] or it may be estimated from imaged volumes that consist primarily of blood.[7]

Forward Transforms	Inverse Transforms
$a_s = \frac{k_{1s}}{2\Delta}(k_{2s} - k_{3s} - k_{4s} + \Delta)$	$k_{1s} = a_s + b_s$
$b_s = \frac{k_{1s}}{2\Delta}(-k_{2s} + k_{3s} + k_{4s} + \Delta)$	$k_{2s} = \frac{a_s c_s + b_s d_s}{a_s + b_s}$
$c_s = \frac{1}{2}(k_{2s} + k_{3s} + k_{4s} + \Delta)$	$k_{3s} = \frac{a_s b_s (c_s - d_s)^2}{(a_s + b_s)(a_s c_s + b_s d_s)}$
$d_s = \frac{1}{2}(k_{2s} + k_{3s} + k_{4s} - \Delta)$	$k_{4s} = \frac{c_s d_s (a_s + b_s)}{a_s c_s + b_s d_s}$
$\Delta = \lvert\sqrt{(k_{2s} + k_{3s} + k_{4s})^2 - 4k_{2s}k_{4s}}\rvert$	

Table 1. Forward and inverse transformations from standard kinetic parameters $[k_{1s}, k_{2s}, k_{3s}, k_{4s}]$ for the voxel s to new parameters $[a_s, b_s, c_s, d_s]$.

Next, we transform the kinetic parameters (k_1, k_2, k_3, k_4) to form the new parameters (a, b, c, d) as shown in Table 1. This transformation is important because while the parameters (a, b, c, d) are well suited for optimization, (k_1, k_2, k_3, k_4) are more physiologically relevant. We use $\varphi_s = [a_s, b_s, c_s, d_s]^t$ to denote the parameter vector for each voxel s.

The total activity concentration (e.g., in nCi/ml) for voxel s at time t is denoted by

$$\begin{aligned} f(\varphi_s, t) &\triangleq (1 - V_B)\left[C_F(s,t) + C_B(s,t)\right] S_A e^{-\lambda t} + V_B C_{WB}(t) \\ &= (1 - V_B)\left[(a_s e^{-c_s t} + b_s e^{-d_s t}) u(t) * C_P(t)\right] S_A e^{-\lambda t} + V_B C_{WB}(t) \end{aligned} \tag{3}$$

where S_A is the initial specific activity of the tracer (nCi/pmol), λ is the decay rate of the isotope (min^{-1}), V_B is a known constant for the volume fraction of the voxel that contains blood, C_{WB} (nCi/ml) is the tracer activity concentration in whole blood (i.e., plasma plus blood cells plus other particulate matter), and $u(t)$ is the unit step function, Let $t_0, \cdots, t_{K-1}$ be the K discrete times at which the tissue is imaged. Then the activity at each time for voxel s is given by the $1 \times K$ row vector $f(\varphi_s) = [f(\varphi_s, t_0), f(\varphi_s, t_1), \cdots, f(\varphi_s, t_{K-1})]$. Let the N voxels be indexed by the values $s = 0, 1, \cdots, N-1$, and let $\varphi = [\varphi_0, \varphi_1, \cdots, \varphi_{N-1}]$ denote the $4 \times N$ matrix of parameters at all voxels. With this, we define the $N \times K$ function, $F(\varphi) = [f(\varphi_0), f(\varphi_1) \cdots, f(\varphi_{N-1}]^t$, which maps the parametric image, φ, to the activity of each voxel at each time. Finally, let $F(\varphi, t_k)$ denote the k^{th} column of $F(\varphi)$, so $F(\varphi, t_k)$ contains the activity for each voxel at time t_k.

3. PARAMETRIC RECONSTRUCTION FROM SINOGRAM DATA

In this section, we describe our method for directly reconstructing the parametric image, φ, from sinogram data. We will do this by first formulating a conventional scanner model under the assumption that the sinogram measurements are Poisson random variables. Once the complete forward model is formulated, we will present an iterative algorithm for computing the maximum a posteriori (MAP) estimate of the parametric image $\hat{\varphi}$ from the sinogram data. Once $\hat{\varphi}$ is computed, the activity images can be computed at any time t simply by evaluating $F(\varphi, t)$ using the kinetic model equations of (3).

3.1. Scanner Model

Let Y_{mk} denote the sinogram measurement for projection $0 \le m < M$ and time frame $0 \le k < K$, and let Y be the $M \times K$ matrix of independent Poisson random variables that form the sinogram measurements. Furthermore, let A be the forward projection matrix, with elements A_{ms} (counts-ml/nCi), and let μ be the number of accidental coincidences. Then the expected number of counts for each measurement at a given time, t_k is given by

$$E[Y_{mk}|F(\varphi, t_k)] = \sum_{s=0}^{N-1} A_{ms} f(\varphi_s, t_k) + \mu \ . \tag{4}$$

It is easily shown that under these assumptions the probability density for the sinogram matrix is given by[8]

$$p(Y|\varphi) = \prod_{k=0}^{K-1} \prod_{m=0}^{M-1} \frac{(A_{m*} F(\varphi, t_k) + \mu)^{Y_{mk}} e^{-(A_{m*} F(\varphi, t_k) + \mu)}}{Y_{mk}!} \tag{5}$$

where A_{m*} is the m^{th} row of the system matrix, A. The log likelihood of the sinogram matrix is then given by

$$LL(Y|\varphi) = \sum_{k=0}^{K-1} \sum_{m=0}^{M-1} Y_{mk} \log(A_{m*}F(\varphi, t_k) + \mu) - (A_{m*}F(\varphi, t_k) + \mu) - \log(Y_{mk}!) \ . \tag{6}$$

This is a very general formulation. For specific scanners, the form of the system matrix A may vary considerably, and accurate determination of the matrix A can be critical to obtaining accurate tomographic reconstructions.[9]

3.2. MAP Estimation Framework

We will use MAP estimation to reconstruct the parametric image. For this purpose, a cost function is formed by negating the log likelihood given in (6) and adding a stabilizing function.

$$C(Y|\varphi) = -LL(Y|\varphi) + S(\varphi) \tag{7}$$

The MAP reconstruction, $\hat{\varphi}$, will be the parametric image that minimizes this cost function.

$$\hat{\varphi} = \arg\min_{\varphi} C(Y|\varphi) \tag{8}$$

The stabilizing function can be obtained from an assumed prior probability distribution for the parametric image. In this work, we model the distribution of the parametric image as a Markov random field (MRF) with a Gibbs distribution of the form

$$p(\varphi) = \frac{1}{z} \exp\{- \sum_{\{s,r\} \in \mathcal{N}} g_{s-r} \|T(\varphi_s) - T(\varphi_r)\|_W^q\} \tag{9}$$

where z is the normalization constant, $\mathcal{N}$ is the set of all neighboring voxel pairs in φ, g_{s-r} is the coefficient linking voxels s and r, q is a constant parameter that controls the smoothness of the edges in the parametric image, $T(\cdot)$ is a transform function, and W is the diagonal weighting matrix.

In this paper, we will assume $q = 2$ and that $\mathcal{N}$ is formed with voxel pairs using an 8-point neighborhood system. In this case, the probability density function corresponds to a Gaussian Markov random field, and we choose the negative logarithm of this function as our stabilizing function.

$$S(\varphi) = \sum_{\{s,r\} \in \mathcal{N}} g_{s-r} \|T(\varphi_s) - T(\varphi_r)\|_W^2 \ . \tag{10}$$

By choosing an appropriate transform function, $T(\cdot)$, the regularization can be done in the space of the physiologically relevant parameters. Typically, we will select $T(\cdot)$ to transform from the a, b, c, d space to the k_1, k_2, k_3, k_4 as show in Table 1; however, any well behaved one-to-one transformation, $T(\cdot)$, is suitable for our algorithm.

3.3. Parametric Image Reconstruction using PICD

The MAP reconstruction described in equation (8) is computed efficiently by an algorithm which we call parametric iterative coordinate descent (PICD). This algorithm is similar to the ICD algorithm used in conventional PET image reconstruction,[8] but it is adapted to account for the nonlinear parameters of the compartmental model. PICD sequentially updates the parameters of each voxel thereby monotonically decreasing the cost function given in Equation (8). When $F(\varphi)$ is a nonlinear function, the PICD algorithm reduces computation by decoupling the dependencies between the compartment model nonlinearities and the forward tomography model.

In order to compute a PICD voxel update, we must compute

$$\varphi_s \leftarrow \arg\min_{\varphi_s} C(Y|\varphi_s) \ . \tag{11}$$

To do this efficiently, we use the second order Taylor expansion of the change in the cost function.

Suppose we are updating the parameters of voxel s from $\varphi_s = [a_s, b_s, c_s, d_s]^t$ to $\tilde{\varphi}_s = [\tilde{a}_s, \tilde{b}_s, \tilde{c}_s, \tilde{d}_s]^t$, and that we represent the change in the time response function of voxel s by the $1 \times K$ vector function, $\Delta f(\tilde{\varphi}_s, \varphi_s) = f(\tilde{\varphi}_s) - f(\varphi_s)$. We next define a simplified cost functional

$$\Delta C(\tilde{\varphi}_s, \varphi_s) \quad = \quad -LL(Y|\tilde{\varphi}_s) + LL(Y|\varphi_s) + \sum_{r \in \partial s} g_{s-r} \|T(\tilde{\varphi}_s) - T(\varphi_r)\|_W^2 \ .$$

Notice that since $\Delta C(\tilde{\varphi}_s, \varphi_s)$ is equal to the change in the cost functional $C(Y|\tilde{\varphi}_s)$ within a constant, so it may be used to compute the voxel update of (11). The value of $\Delta C(\tilde{\varphi}_s, \varphi_s)$ can then be locally approximated with a second order Taylor series as

$$\Delta C(\tilde{\varphi}_s, \varphi_s) \quad \approx \quad \Delta f(\tilde{\varphi}_s, \varphi_s)\theta_1 + \frac{1}{2} \|\Delta f(\tilde{\varphi}_s, \varphi_s)\|_{\theta_2}^2 + \sum_{r \in \partial s} g_{s-r} \|T(\tilde{\varphi}_s) - T(\varphi_r)\|_W^2$$

where ∂s denotes the set of voxels that are 8-neighbors of voxel s, θ_1 is a $K \times 1$ vector, θ_2 is a $K \times K$ diagonal matrix, and $\|x\|_{\theta_2}^2 = x^t \theta_2 x$. Here the values of θ_1 and θ_2 consist of the first and second derivatives respectively of the log likelihood function evaluated at each time frame. These derivatives at time frame k can be iteratively updated using the equations of the conventional iterative coordinate descent (ICD) algorithm,[8] given in (12) and (13).

$$[\theta_1]_k \leftarrow \sum_{m=0}^{M-1} A_{ms} \left(1 - \frac{Y_{mk}}{A_{m*} F(\varphi, t_k) + \mu} \right) \tag{12}$$

$$[\theta_2]_{k,k} \leftarrow \sum_{m=0}^{M-1} Y_{mk} \left(\frac{A_{ms}}{A_{m*} F(\varphi, t_k) + \mu} \right)^2 \tag{13}$$

Then the PICD update can then be expressed as

$$\tilde{\varphi}_s \leftarrow \arg\min_{\tilde{\varphi}_s} \left\{ \Delta f(\tilde{\varphi}_s, \varphi_s)\theta_1 + \frac{1}{2} \|\Delta f(\tilde{\varphi}_s, \varphi_s)\|_{\theta_2}^2 + \sum_{r \in \partial s} g_{s-r} \|T(\tilde{\varphi}_s) - T(\varphi_r)\|_W^2 \right\} \tag{14}$$

where $\Delta f(\tilde{\varphi}_s, \varphi_s) = f(\tilde{\varphi}) - f(\varphi)$. We have found that the PICD update is best implemented using two-stage nested optimization.

$$(c_s, d_s) \leftarrow \arg \min_{\tilde{c}_s \geq \tilde{d}_s \geq 0} \left\{ \arg \min_{\tilde{a}_s, \tilde{b}_s \geq 0} \left\{ \Delta C([\tilde{a}_s, \tilde{b}_s, \tilde{c}_s, \tilde{d}_s], \varphi_s) \right\} \right\} \ . \tag{15}$$

This nested optimization strategy is very important in reducing computation and assuring robust convergence. The inner optimization over $\tilde{a}_s$ and $\tilde{b}_s$ must be performed many times since this result is required for each update of outer optimization over $\tilde{c}_s$ and $\tilde{d}_s$. Fortunately, optimization over $\tilde{a}_s$ and $\tilde{b}_s$ can be done very efficiently with a simple steepest descent algorithm because this optimization does not require updating of θ_1, θ_2, $\alpha(\tilde{c}_s)$, or $\beta(\tilde{d}_s)$. Optimization with respect to $(\tilde{c}_s, \tilde{d}_s)$ is done using iterative 1-D golden section search along the $\tilde{c}_s$ and $\tilde{c}_s + \tilde{d}_s$ directions. This method assures the convergence is to a local minimum that meets the Kuhn-Tucker conditions.[10]

3.4. Multiresolution Initialization

It is well known that for the tomographic problem the ICD reconstruction algorithm tends to have slow convergence at low spatial frequencies.[11] To solve this problem, we use a multiresolution reconstruction scheme, which first computes coarse resolution reconstructions and then and proceeds to finer scales. The coarsest resolution reconstruction is initialized with a single set of parameters obtained by weighted least squares curve fitting to the average emission rate of each time frame. Importantly, the average activity of each time frame can be calculated directly from the sinogram data with little computation. Finer resolution reconstructions are then initialized by interpolating the parametric reconstruction of the previous coarser resolution. This recursive process reduces computation because the computationally inexpensive reconstructions at coarse levels provide a good initialization for finer resolution reconstructions.

4. IMAGE DOMAIN PARAMETER ESTIMATION METHODS

For purposes of comparison, we will also consider image domain methods which estimate parameters at each voxel from reconstructed images at each time. Each of these methods requires that the sinogram at each time frame be reconstructed using conventional reconstruction methods. For these methods, let $x_s(t_k)$ denote the reconstructed activity of voxel s at time frame k collected at time t_k, and let $x_s = [x_s(t_0), x_s(t_1), \cdots, x_s(t_{K-1})]$ denote the activity of voxel s at all time frames.

4.1. Pixel-wise Weighted Least Square (PWLS) Method

The pixel-wise weighted least squares method estimates the parameters of each voxel by iteratively minimizing the weighted square error between the reconstructed time response of the voxel and the model output.

The parameters of voxel s are estimated as

$$\hat{\varphi}_s = \arg\min_{\varphi_s} \|x_s - f(\varphi_s)\|^2_{W_s} \tag{16}$$

where W_s is the $K \times K$ diagonal weighting matrix for voxel s. The weight of each time frame is chosen to be inversely proportional to the variance of the voxel activity in that time frame. This variance can be approximated by the activity estimate of this voxel, normalized by the duration of the time frame. In this case, W_s is a diagonal matrix with diagonal elements given by $[W_s]_{k,k} = \frac{\Delta t_k}{\max\{x_{MIN}, x_s(t_k)\}}$, where Δt_k is the duration of time frame k, and x_{MIN} controls the maximum allowable value for the weights. The parameters are estimated using the same nested optimization strategy as specified in equation (15).

4.2. Pixel-wise Weighted Least Square Method with Spatial Regularization

The spatial variation of the PWLS parameter estimates can be reduced by adding a stabilizing function to equation (16). The resulting estimate is given by

$$\hat{\varphi} = \arg\min_{\varphi} \sum_{s=0}^{N-1} \|x_s - f(\varphi_s)\|^2_{W_s} + S(\varphi) \tag{17}$$

where $S(\cdot)$ is the spatial stabilizing functional.[12, 13]

In the first method, which we call the pixel-wise least squares regularized (PWLSR) method, the stabilizing function has the form specified in equation (10). This is the same stabilizing function as was used for direct parametric reconstruction. For the second method, which we call the PWLSZ method, we implemented the stabilizing functional described in.[12] This method smooths the PWLS estimate and uses it in the stabilizing function. For both of these methods the solution to (17) is computed using the nested optimization strategy specified in (15).

4.3. Linear (Logan) Method

Kinetic parameter groups can sometimes be easily estimated by properly transforming the data. The Logan plot is a popular integral transform of the model given in equations (1), (2), and (3). This transformation can be expressed as follows.

$$\left[\frac{\int_0^{t_k} x_s(t)dt}{x_s(t_k)}\right] = \frac{k_{1s}}{k_{2s}}\left(1 + \frac{k_{3s}}{k_{4s}}\right)\left[\frac{\int_0^{t_k} C_P(t)dt}{x_s(t_k)}\right] + const\ . \tag{18}$$

When the transformed variables (quantities in square brackets above) are plotted against each other, the resulting line has a slope equal to the compound parameter VD_s.

To calculate BP_s the brain is segmented into a target region and a reference region. The target region consists of voxels within the brain that contain receptors for the tracer; and the reference region consists of the voxels that do not contain receptors for the tracer (i.e. $k_3 = 0$). Let, $\mathcal{T}$ be the set of voxel indices from target region, and $\mathcal{R}$ be the set of voxel indices from reference region.

For a voxel $r \in \mathcal{R}$ (from reference region), the distribution volume is $VD_r = \frac{k_{1r}}{k_{2r}}, \quad r \in \mathcal{R}$. For each voxel $s \in \mathcal{T}$ (from target region), the distribution volume ratio is $DVR_s = 1 + \frac{k_{3s}}{k_{4s}}$, where $|\mathcal{R}|$ denotes the number of voxels in the region $\mathcal{R}$. Hence, the binding potential for the target region can be calculated as $BP_s = DVR_s - 1$.

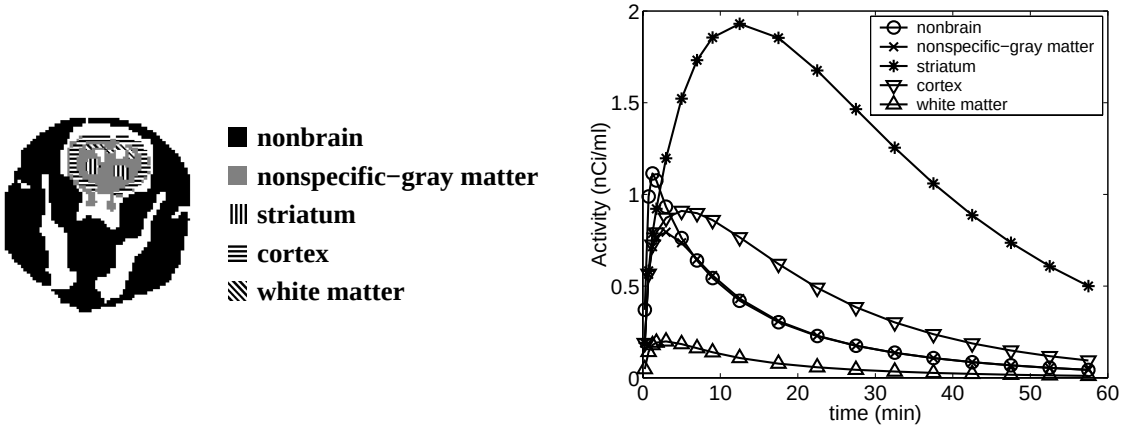

(a) (b)

Figure 2. (a) Regions of the rat phantom derived from a segmented MR Image. (b) Time-activity curves for 5 distinct tissue regions in rat brain phantom.

Region	k_1 min^{-1}	k_2 min^{-1}	k_3 min^{-1}	k_4 min^{-1}	a min^{-1}	b min^{-1}	c min^{-1}	d min^{-1}
Background	0	0	0	0	0	0	0	0
CSF	0	0	0	0	0	0	0	0
Nonbrain	.1836	.8968	0	0	.1836	0	.8968	0
Nonspecific-gray matter	.0918	.4484	0	0	.0918	0	.4484	0
Striatum	.0918	.4484	1.2408	.1363	.02164	.07016	1.7914	.0312
Cortex	.0918	.4484	.141	.1363	.0607	.0311	.628	.09725
White matter	.02295	.4484	0	0	.02295	0	.4484	0

Table 2. Kinetic parameters used in the simulations for distinct tissue regions of the rat head.

5. SIMULATIONS

The following section compares the accuracy and computational burden of direct parametric reconstruction and image domain estimation methods.

5.1. Phantom Design

Our simulation experiments are based on a phantom of a rat's head. Figure 2(a) shows a schematic representation of the rat phantom and its constituent regions. The phantom has 7 regions including the background. These regions were obtained by segmenting an MRI scan of a rat through automated and manual techniques.[14] The regions and their corresponding parameters[15] are given in Table 2, and their time activity curves are shown in Fig. 2(b). Time frames of emission images are generated using these parameter images and the 2-tissue compartment model equations, and the plasma function, $C_P(t)$, is generated using equation (2) from reference.[16] The blood contribution to the PET activity is assumed to be zero, and the tracer is assumed to be raclopride with ^{11}C, which has a decay constant of $\lambda = 0.034$ min^{-1}. Total scan time is 60 min., divided into 18 time frames with 4×0.5 min, 4×2 min, and 10×5 min. The phantom had a resolution of 128×128 with each voxel having dimensions of (1.2 mm)^3.

The rat phantom image at each time frame is forward projected into a sinogram using a Poisson model for the detected counts with a background (accidental coincidence) level of 0.001nCi/ml. Each sinogram consists of 180 angles and 200 radial bins per angle. A triangular point spread function with a 4 mm base width is used in forward projections. The blood function, $C_P(t)$ is scaled so that the total number of counts in all sinogram frames is approximately 10 million.

5.2. Algorithm Implementation

Direct reconstructions were computed using the PICD algorithm with three levels of multiresolution optimization corresponding to resolutions of 32×32, 64×64 and 128×128.

The maximum likelihood (ML) estimate of $\sigma^2_{k_i}$ was computed for each parameter from the original parametric image as described in Saquib *et al.*[17] These ML parameters are then linearly scaled all together to find a set of regularization parameters that minimize the RMSE of the estimated kinetic parameters. The resulting diagonal weighting matrix, W, from equation (10) has diagonal entries given by $W_{i,i} = \beta \frac{1}{2\sigma^2_{k_i}}$ where β is the scaling factor that minimizes the parameter RMSE. Some results use regularization in the k_1, k_2, BP, and VD parameters. In this case, scaling parameters are selected similarly using the appropriate parameter values.

The image domain parameter estimation methods of section 4 require that the image be reconstructed for each time frame. For this purpose, we used MAP image reconstruction with a quadratic prior and a single fixed regularization parameter for all frame times. This single fixed parameter was chosen to minimize the total mean square error of the reconstructed emission image frames.

For the linear (Logan) method, the cortex and striatum regions are selected as target regions, and the nonspecific-gray matter was used as the reference region. Since these regions were selected precisely from simulated data, all assumptions of this method are perfectly satisfied.

A fixed number of iterations is used for each method. The multiresolution PICD method uses 30 iterations at 32×32 resolution, 20 iterations at 64×64 resolution, and 20 iterations at 128×128 resolution. Image domain methods use 15 iterations.

5.3. Results

Figure 3 shows the reconstructions of the kinetic parameters. The first row contains the original parametric images. The remaining rows are respectively the reconstructions of PWLS, PWLSZ, PWLSR, PICD reconstruction regularized on k_1, k_2, k_3, and k_4, and PICD reconstruction regularized on k_1, k_2, BP, and VD.* In addition, the normalized RMSE of parameters k_1, k_2, k_3, and k_4 estimated by these algorithms are listed in Fig. 5(a). The RMSE of k_1 is calculated over the whole image. The RMSE of parameters k_2 and k_3 are calculated over the support of k_1, and the RMSE of k_4 is calculated over the support of k_3.

For the nonlinear parameters k_3 and k_4, the PWLS and PWLSZ methods both produced reconstructions which are very noisy, and this is reflected in the RMSE calculations. The PWLSR method with the GMRF prior produces lower RMSE reconstructions with more visually acceptable results for k_3 and k_4; however some details in these nonlinear parameters are lost. The parametric reconstruction regularized on k_1, k_2, k_3, and k_4 produces higher SNR reconstructions than any of the image domain methods, and the reconstructed images are visually similar to the original phantom. However, the parametric reconstructions with regularization on k_1, k_2, BP, and VD yield the best quality results judging from both the visual quality and the computed RMSE.

For the comparison of parameters BP and VD, spatial regularization is applied on k_1, k_2, BP, and VD. In this case, the scaling of the four regularization constants are chosen to minimize the RMSE of the BP and VD estimates alone. The results are shown in Fig. 4 and the normalized RMSE of the estimates of all methods are given in Fig. 5(b). The RMSE of BP is estimated over the support of k_3, and the RMSE of VD is estimated over the support of k_1. Again, parametric image reconstruction produces the lowest RMSE estimation for both BP and VD.

Once the parametric image is reconstructed, the ODE's can be solved for any particular time to reconstruct the corresponding emission image. Fig. 6 compares these reconstructions to the conventional reconstructions computed using FBP and MAP reconstruction for time frames 5, 10, and 15. The FBP reconstructions use a Hamming filter with cutoff at the Nyquist frequency. The RMSE of these reconstructions for each frame and for total RMSE of all frames are given in Fig. 7(a).

Finally, the convergence speed as a function of CPU time for all algorithms is given in Fig. 7(b). The time needed to reconstruct emission images required by image domain methods is included in this figure. As can be

*A very small amount of regularization was also used for k_3 and k_4 (i.e. $\sigma^2_{k_3} = 1\text{min}^{-2}$ $\sigma^2_{k_4} = 0.1\text{min}^{-2}$) to suppress impulsive noise in these reconstructions.

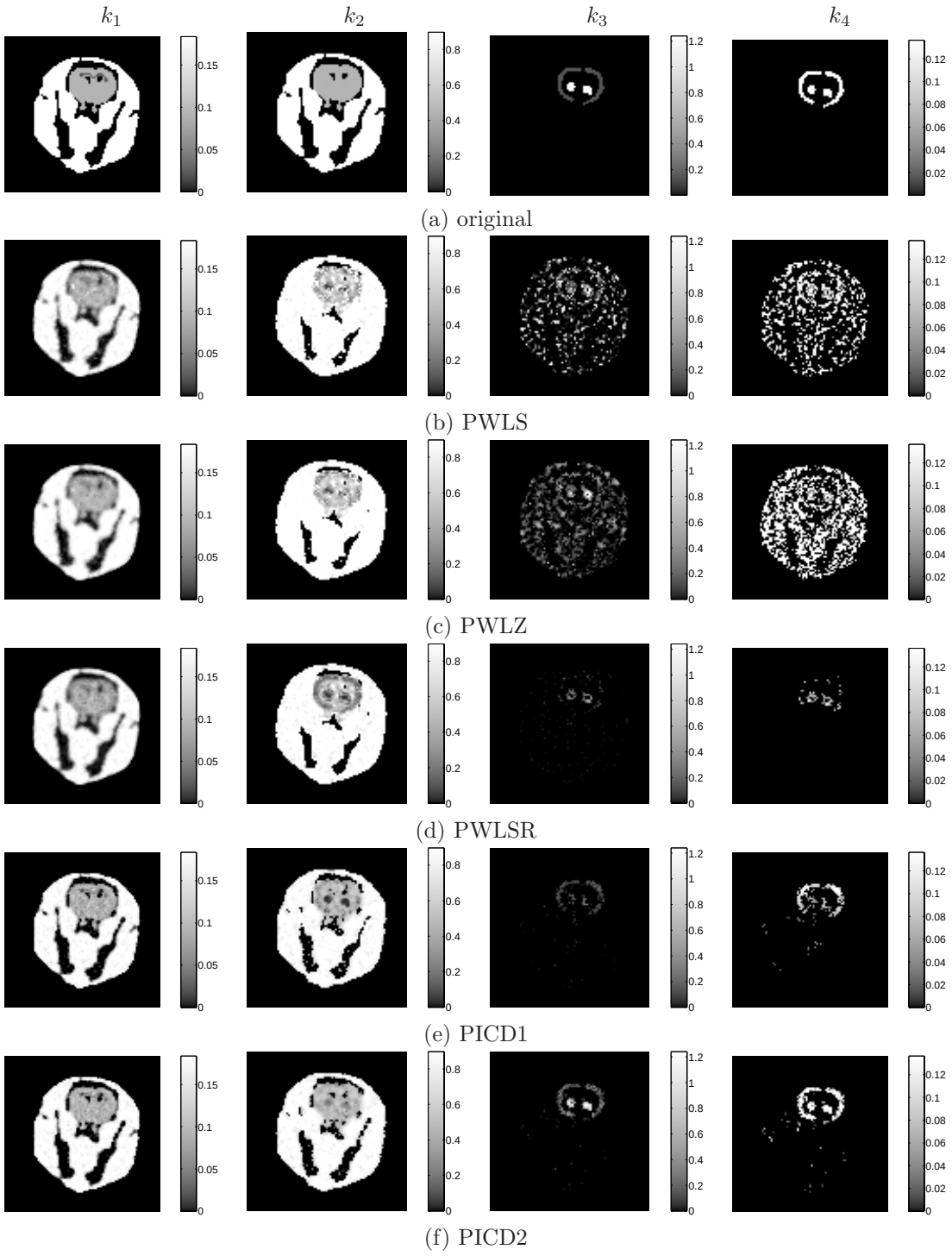

Figure 3. Parametric images of k_1, k_2, k_3 and k_4 estimated by the algorithms; (a) original (b) PWLS (c) PWLSZ (d) PWLSR (e) PICD1: PICD reconstruction (new method) regularized on k_1, k_2, k_3, and k_4 (f) PICD2: PICD reconstruction (new method) regularized on k_1, k_2, BP, and VD.

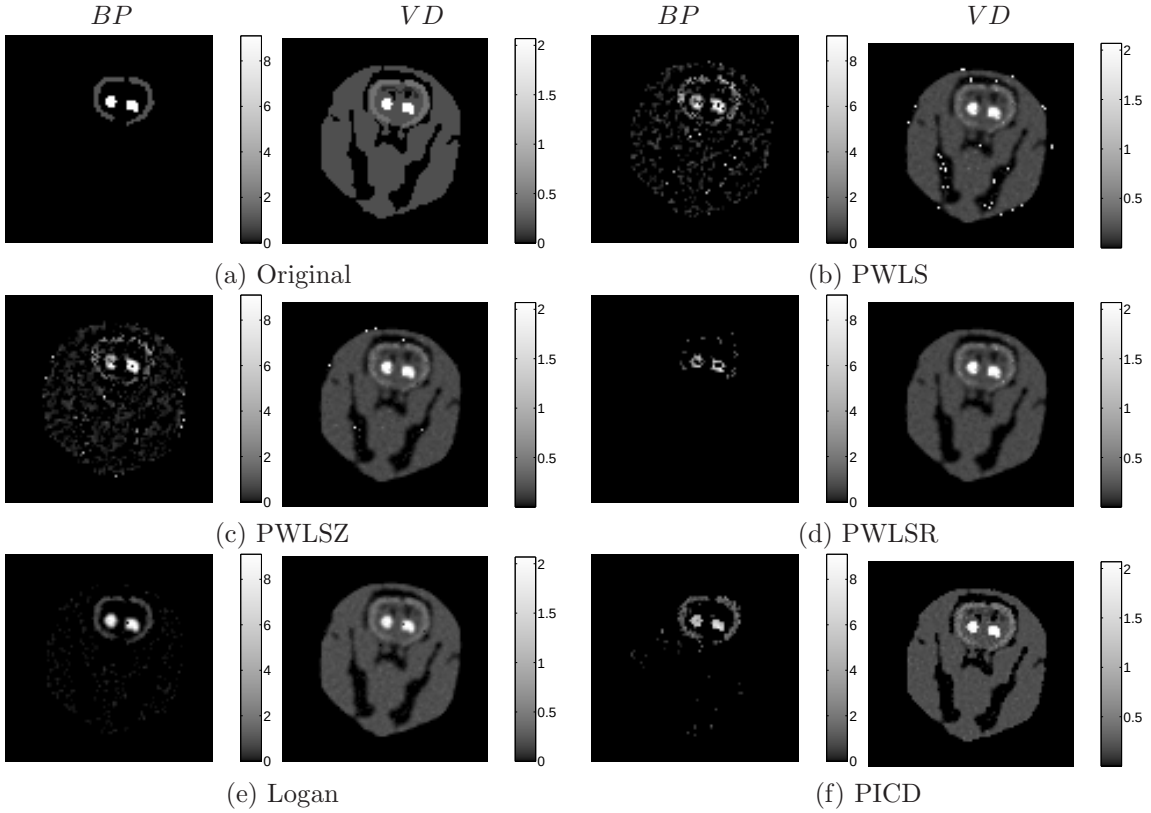

Figure 4. Parametric images of BP and VD estimated by the algorithms; a) original (b) PWLS (c)PWLSZ (d) PWLSR (e) Logan (f) PICD reconstruction (new method).

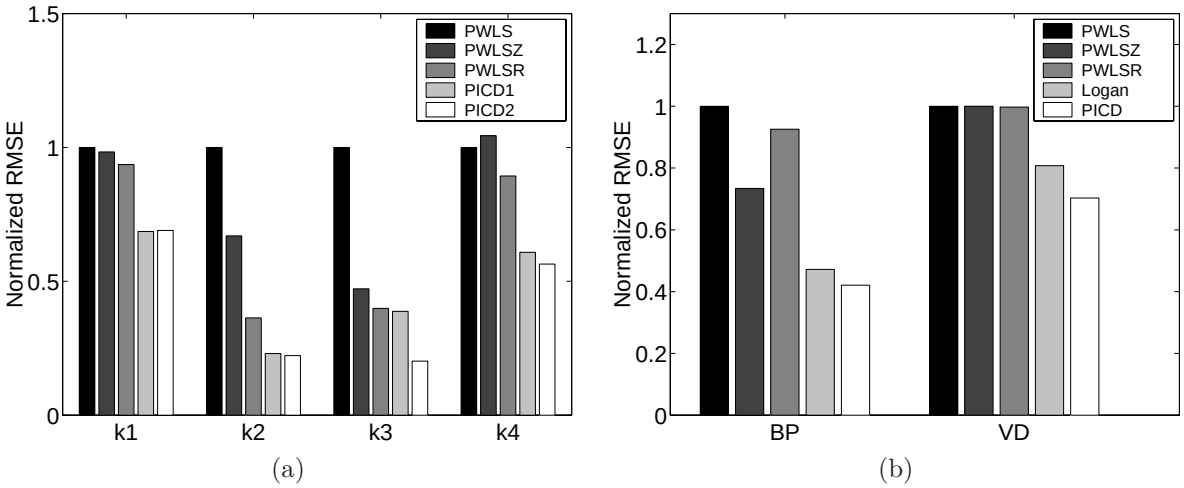

Figure 5. (a) Normalized RMSE for the reconstructed parametric images, k_1, k_2, k_3, and k_4 . PICD1 denotes the PICD reconstruction regularized on k_1, k_2, k_3, and k_4. PICD2 denotes the PICD reconstruction regularized on k_1, k_2, BP, and VD. (b) Normalized RMSE for the reconstructed BP and VD. PICD reconstruction uses regularization on k_1, k_2, BP, and VD.

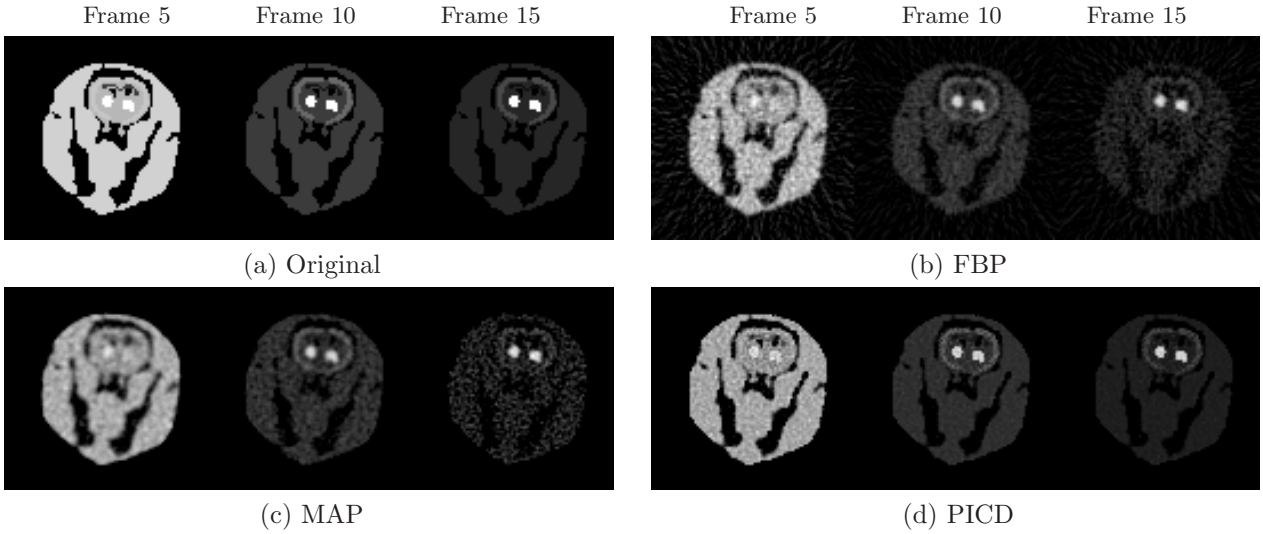

Figure 6. Activity images (a) original phantom (b) FBP reconstruction (c) MAP (d) PICD reconstruction (new method) for frames 5, 10, and 15.

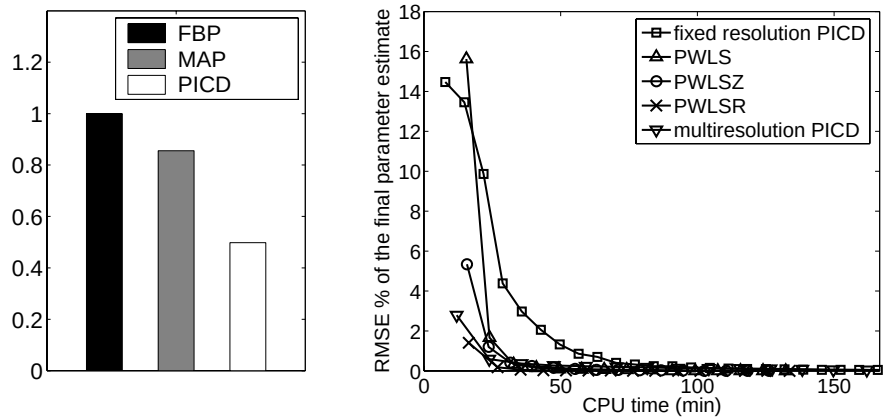

Figure 7. (a) Normalized total RMSE of emission image reconstructions. (b) Convergence curves for the estimation algorithms.

seen from this figure, the convergence speed of direct parametric reconstruction is comparable to the pixel-wise methods.

6. CONCLUSIONS

In this paper, we introduce a method for the direct reconstruction of kinetic parameters at each voxel from dynamic PET sinogram data. Our algorithm, which we call parametric iterative coordinate decent (PICD), decouples the nonlinearities between the tomographic model, the kinetic model, and the regularized parameters. It also allows one to regularize with respect any desired parametrization, even if the parameters that are selected are nonlinearly related to the projections or the kinetic model parameters. Using an anatomically and physiologically realistic small animal phantom, we demonstrated that our method can reduce the mean squared error in model parameter estimates; and we show that for our example, it does not require substantially more computation than more conventional methods for computing dense parameter estimates in the image domain.

Acknowledgement

Authors would like to thank Cristian Constantinescu, Chunzhi Wang, Dr. Karmen Yoder and Dr. Ti-Qiang Li at Indiana University School of Medicine for their help in constructing the rat phantom from MR data.

REFERENCES

1. R. E. Carson and K. Lange, "The EM parametric image reconstruction algorithm," *Journal of the American Statistical Association* **80**(389), pp. 20–22, 1985.
2. M. Kamasak, C. A. Bouman, E. D. Morris, and K. Sauer, "Direct reconstruction of kinetic parameter images from dynamic PET data," in *Proceedings of 37th Asilomar Conference on Signals, Systems and Computers*, pp. 1919–1923, (Pacific Grove, CA), November 9-12 2003.
3. M. E. Kamasak, C. A. Bouman, E. D. Morris, and K. Sauer, "Direct reconstruction of kinetic parameter images from dynamic PET data," *IEEE Trans. on Medical Imaging* , to appear.
4. S. C. Huang and M. E. Phelps, "Principles of tracer kinetic modeling in positron emission tomography," in *Positron Emission Tomography and Autoradiography*, M. E. Phelps, J. Mazziotta, and H. Schelbert, eds., pp. 287–346, Raven Press, New York, 1986.
5. E. D. Morris, C. J. Endres, K. C. Schmidt, B. T. Christian, R. F. Muzic Jr., and R. E. Fisher, "Kinetic modeling in PET," in *Emission Tomography: The Fundamentals of PET and SPECT*, M. Wernick and J. Aarsvold, eds., ch. 23, Academic Press, San Diego, 2004.
6. R. E. Carson, "Tracer kinetic modeling in PET," in *Positron Emission Tomography, Basic Science and Clinical Practice*, P. E. Valk, D. L. Bailey, D. W. Townsend, and M. N. Maisey, eds., Springer, London, 2002.
7. M. Liptrot, K. H. Adams, L. Martiny, L. H. Pinborg, M. N. Lonsdale, N. V. Olsen, S. Holm, C. Svarer, and G. M. Knudsen, "Cluster analysis in kinetic modelling of the brain: a noninvasive alternative to arterial sampling," *NeuroImage* **21**(2), pp. 483–493, 2004.
8. C. A. Bouman and K. Sauer, "A unified approach to statistical tomography using coordinate descent optimization," *IEEE Trans. on Image Processing* **5**, pp. 480–492, March 1996.
9. E. Mumcuoglu, R. M. Leahy, S. Cherry, and E. Hoffman, "Accurate geometric and physical response modeling for statistical image reconstruction in high resolution PET scanners," in *Proceedings of IEEE Nuclear Science Symposium and Medical Imaging Conference*, pp. 1569–1573, 1996.
10. H. W. Kuhn and A. W. Tucker, "Nonlinear programming," in *Proceedings of 2nd Berkeley Symposium on Mathematical Statistics and Probabilistics*, pp. 481–492, University of California Press, 1951.
11. K. Sauer and C. A. Bouman, "A local update strategy for iterative reconstruction from projections," *IEEE Trans. on Signal Processing* **41**, pp. 534–548, February 1993.
12. S. C. Huang and Y. Zhou, "Spatially-coordinated regression for image-wise model fitting to dynamic PET data for generating parametric images," *IEEE Trans. on Nuclear Science* **45**, pp. 1194–1199, June 1998.
13. F. O'Sullivan and A. Saha, "Use of ridge regression for improved estimation of kinetic constants from PET data," *IEEE Trans. on Medical Imaging* **18**, pp. 115–125, February 1999.
14. G. Paxinos and C. Watson, *The Rat Brain in Stereotaxic Coordinates*, Academic Press, 4th ed., 1998.
15. S. Pappata, S. Dehaene, J. B. Poline, M. C. Gregoire, A. Jobert, J. Delforge, V. Frouin, M. Bottlaender, F. Dolle, L. D. Giamberardino, and A. Syrota, "In vivo detection of striatal dopamine release during reward: a PET study with [^{11}C]raclopride and a single dynamic scan approach," *Neuroimage* **16**(4), pp. 1015–1027, 2002.
16. K.-P. Wong, D. Feng, S. R. Meikle, and M. J. Fulham, "Simultaneous estimation of physiological parameters and the input function - in *vivo* PET data," *IEEE Transactions on Information Technology in Biomedicine* **5**, pp. 67–76, March 2001.
17. S. S. Saquib, C. A. Bouman, and K. Sauer, "ML parameter estimation for Markov random fields with applications to Bayesian tomography," *IEEE Trans. on Image Processing* **7**, pp. 1029–1044, July 1998.